Condensed Matter Physics, 1999, Vol. 2, No. 1(17), p. 93–108

CONDENSED MATTER PHYSICS

Lattice dynamics of a monoclinic CsH_2PO_4 crystal

Ya.I.Shchur [1], R.R.Levitskii [2], O.G.Vlokh [1], A.V.Kityk [1], Y.M.Vysochansky [3], A.A.Grabar [3]

[1] Institute of Physical Optics,
23 Dragomanov Str., 290005 Lviv, Ukraine

[2] Institute for Condensed Matter Physics
of the National Academy of Sciences of Ukraine,
1 Svientsitskii Str., 290011 Lviv, Ukraine

[3] Uzhgorod State University,
46 Pidhirna Str., 294000 Uzhgorod, Ukraine

Received November 19, 1997

The phonon dispersion relations in a CsH_2PO_4 crystal in a paraelectric phase by means of a rigid molecular-ion model are calculated. The phonon spectra in the quasi-harmonic approximation at various values of temperature and hydrostatic pressure are obtained. The condensation of A_u external phonon branch in the centre and at the boundary of the Brillouin zone is obtained.

Key words: *lattice dynamics, soft mode, structural phase transition, phonon spectrum*

PACS: *63.20.-e, 63.20.Dj*

1. Introduction

Caesium dihydrogen phosphate CsH_2PO_4 (CDP) belongs to a group of monoclinic phosphates of the KH_2PO_4-type, like KD_2PO_4 (DKDP), RbD_2PO_4 (DRDP), TlH_2PO_4 (TDP), $RbHPO_4$ (LHP). Owing to their interesting properties, the CDP crystal and its deuterated analogue CsD_2PO_4 (DCDP) have been intensively studied by X-ray diffraction [11, 21, 34], neutron scattering [9, 12, 22, 33], dielectric [5,7, 31] acoustic [1, 14, 24], Raman scattering [8, 13, 20, 38], hyper-Raman scattering [28], IR absorption [30] and optic [35] measurements. However, a lattice dynamics of the CDP crystal in the region of phase transitions (PTs) and a triple point have been investigated insufficiently.

In this paper a theoretical treatment of the lattice dynamics of CDP within the framework of a rigid molecular-ion model in the quasi-harmonic approximation

in paraelectric (PE) phase under the influence of hydrostatic pressure and temperature is presented. We restrict ourselves to the consideration of low-frequency external phonon modes which gives the most complete information about the nature of PTs. Moreover, in monoclinic phosphates of the CDP-type the PTs are often accompanied by unit cell multiplication (e.g., in DRDP [10, 29] and TDP [2, 26] crystals). Therefore, the use of a CDP crystal as a model object for the investigation of structural PTs seems to the quite reasonable.

2. Structure and symmetry

In a high-temperature PE phase the CDP crystal has a space group $P2_1/m$ with two molecules per unit cell ($a = 7.906A, b = 6.372A, c = 4.883A, \beta = 107.73^o$ [21]). The CDP crystal structure is depicted in figure 1 (according to [9]). The peculiarity of this structure is the presence of two types of hydrogen bonds O–H...O. The shorter bonds (R = 2.47 Å) link the PO_4 groups into zig-zag-like chains running along the b axis. In the PE phase the protons are disordered on those bonds. The longer bonds (R = 2.54 Å), which are directed approximately along the c axis, cross-link the chains to form (b, c) layers. The protons on the longer bonds are ordered on one of the two possible equilibrium sites at all temperatures.

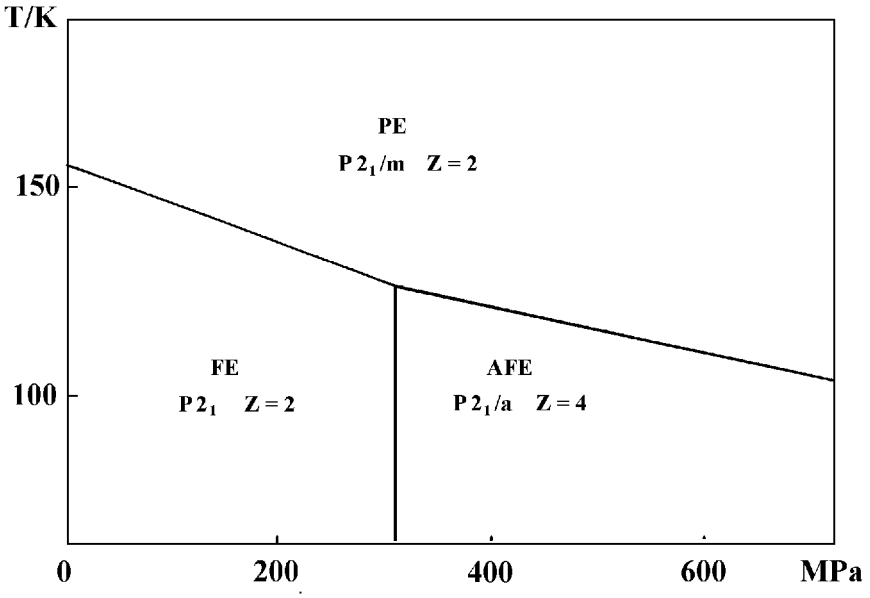

Figure 1. The P-T phase diagram of a CsH_2PO_4 crystal in the PE phase (according to [20]).

At T_c = 156 K and atmospheric pressure, a CDP crystal undergoes the PT into the PE phase with the space group $P2_1$ and the spontaneous polarization $P_s \| b$ ($Z = 2$, a = 7.87 Å, b = 6.32 Å, c = 4.89 Å, $\beta = 108.3^o$ at T = 83 K [12]). In the PE phase a proton ordering on the shorter hydrogen bonds occurs.

By means of the dielectric [32] and neutron [25] investigation, it was shown that at some values of hydrostatic pressure and temperature, the PT into the antifer-

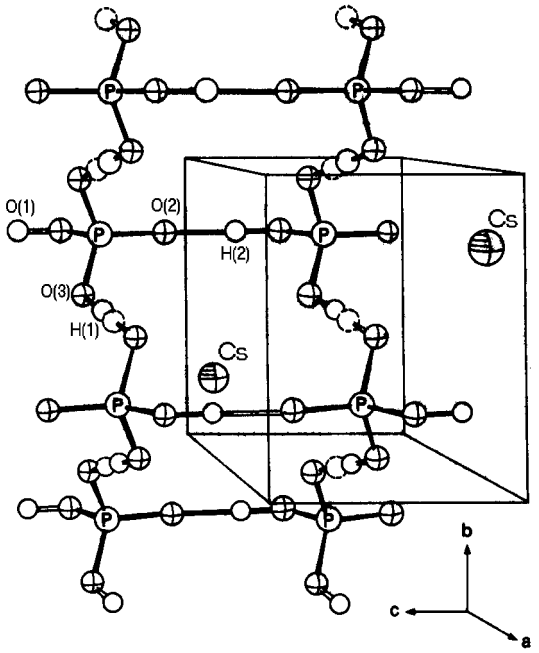

Figure 2. The structure of a CsH_2PO_4 crystal in the PE phase (according to [9]).

roelectric (AFE) phase takes place in a CDP crystal. The pressure-temperature phase diagram of a CDP crystal is depicted in figure 2 [21]. The neutron scattering study [25] has revealed that the PT into the AFE phase is accompanied by a unit cell doubling along the a axis ($Z = 4$, $a = 15.625$Å, $b = 6.254$Å, $c = 4.886$Å, $\beta = 108.08^o$). The antiparallel ordering of protons on the neighbouring chains running along the b axis takes place. The atom coordinates determined by [25] allowed the authors to identify the symmetry of the AFE phase both with the $P2_1$ space group and with the $P2_1/a$ one. Due to the Raman spectra studies of the DCDP crystal at $T = 83$ K and $P = 800$ MPa [20] a conclusion was drawn that the symmetry of the AFE phase is $P2_1/a$. Besides, as it follows from the general symmetry consideration (Curie principle [3]), if there is an inversion centre in the PE phase, it must persist in the AFE phase, too. We shall assume that in the AFE phase the $P2_1/a$ symmetry is realized. For the lattice dynamics consideration, an orthonormal set of axes X, Y and Z was used. In the PE phase, the principal parameters of the monoclinic lattice mP with respect to the orthonormal axes are the following:

$$\boldsymbol{a} = (0, \tau_y, 0), \quad \boldsymbol{b} = (0, 0, \tau_z), \quad \boldsymbol{c} = (\tau \cos\alpha, -\tau \sin\alpha, 0), \tag{1}$$

where $\tau = c; \tau_y, \tau_z$ are the corresponding principal parameters along the Y and Z axes; $\alpha = 17.73^o$. At the same time, the reciprocal lattice parameters can be written as

$$\begin{aligned} &\boldsymbol{b}_1 = (2\pi \tan\alpha/\tau_y, 2\pi/\tau_y, 0), \quad \boldsymbol{b}_2 = (0, 0, 2\pi/\tau_z), \\ &\boldsymbol{b}_3 = (2\pi/(\tau\cos\alpha), 0, 0). \end{aligned} \tag{2}$$

3. Group-theoretical classification of lattice vibrations

A general group theory analysis of the normal modes of a CDP crystal in the PE phase for 14 wavevectors $\boldsymbol{q}$ which correspond to all the symmetrical points and lines of the Brillouin zone (BZ) of the monoclinic lattice mP was made. A symmetrized form of the dynamical matrix $D(\boldsymbol{q})$, the matrices of irreducible multiplier representations (IMRs) $T(\boldsymbol{q}, h)$ (here h is an element of the wavevector point group $G_0(\boldsymbol{q})$) and the symmetry vectors $E(\boldsymbol{q})$ for wavevectors $\boldsymbol{q}_i (i = 1, 14)$ were obtained. However, in this work we present the results for the most interesting from the physical point of view cases $(\boldsymbol{q}_7, \boldsymbol{q}_1, \boldsymbol{q}_{12}, \boldsymbol{q}_{13}, \boldsymbol{q}_3, \boldsymbol{q}_{11})$ which will be used in numerical calculations. Kovalev's notation [15] was used for the identification of wavevectors, elements of the wavevector point groups $G_0(\boldsymbol{q})$, symmetrical points and lines of the BZ.

We carried out the lattice dynamics study of a CDP crystal within the rigid molecular-ion approximation [36] where the H_2PO_4 groups are treated as rigid and nondeformable. Hence, there are two Cs^+ ions ($k = 1, 2$) and two $(H_2PO_4)^-$ ions ($k = 3, 4$) in the unit cell of a CDP crystal. In this case, there are 18 external branches in the phonon spectrum of a CDP crystal.

The symmetry vectors in the centre of the BZ ($\boldsymbol{q}_7 = 0$) corresponding to the translational displacements and librations of the structural units of the crystal are given in table 1. They are used for diagonalization of the dynamical matrix and phonon frequencies classification according to IMRs. The point groups of the wavevectors ($\boldsymbol{q}_7$, $\boldsymbol{q}_1$, $\boldsymbol{q}_{12}$, $\boldsymbol{q}_{13}$, $\boldsymbol{q}_3$, $\boldsymbol{q}_{11}$) and normal modes classification by the IMRs of these groups are shown in table 2. The IMRs of the above mentioned groups are given in table 3.

4. Model

The crystal potential energy Φ in the rigid molecular-ion approximation is written as [6]

$$\Phi = \frac{1}{2} \sum_{\substack{l,k \\ k \subset K}} \sum_{\substack{l',k' \\ k' \subset K'}} \frac{1}{4\pi\varepsilon_0} \frac{Z_{Kk} Z_{K'k'} e^2}{r(lKk, l'K'k')} + a \exp\left\{ -\frac{br(lKk, l'K'k')}{R(k) + R(k')} \right\}, \qquad (3)$$

where $a = 1822$ eV, $b = 12.364$; l, l' are unit cell indices; K, K' are the indices of atomic or molecular vibrating units in the unit cell; k, k' are the indices of atoms in molecular units; $k \subset K$ means that atom k belongs to molecule K; e is an electron charge; Z_{Kk} and R_{Kk} are effective charge and radii parameters of Kk atom, respectively; r is a distance between Kk and $K'k'$ atoms. The first and second terms of expression (3) represent the long-range Coulomb and the short-range Born-Mayer-type repulsive energy, respectively. Moreover, we assumed that the total potential energy is a sum of the pair interactions of the atoms of different molecules. Interactions between the atoms within a molecule have been neglected.

The unknown parameters Z_{Kk} and R_{Kk} are determined from the lattice equilibrium conditions with respect to any macroscopic internal strains [4] and also

Table 1. Symmetry vectors for CsH_2PO_4 in the PE phase in the centre of the BZ ($\boldsymbol{q}_7 = 0$). Designations x, y and z refer to the translations along the X, Y and Z axes; $\tilde{x}, \tilde{y}$ and $\tilde{z}$ refer to the librations about X, Y and Z axes.

Representation	Symmetry vectors
A_g	$x(1)-x(2), y(1)-y(2), x(3)-x(4), y(3)-y(4),$ $\tilde{z}(3)+\tilde{z}(4)$
B_g	$z(1)-z(2), z(3)-z(4), \tilde{x}(3)+\tilde{x}(4), \tilde{y}(3)+\tilde{y}(4)$
A_u	$z(1)+z(2), z(3)+z(4), \tilde{x}(3)-\tilde{x}(4), \tilde{y}(3)-\tilde{y}(4)$
B_u	$x(1)+x(2), y(1)+y(2), x(3)+x(4), y(3)+y(4),$ $\tilde{z}(3)-\tilde{z}(4)$

Table 2. Point groups of wavevectors and classification of normal modes for CsH_2PO_4 ($-\frac{1}{2} < \mu_1,\ \mu_2,\ \mu_3 < \frac{1}{2}$) in the PE phase.

Wavevector	Point group $G_0(\boldsymbol{q})$ of wavevector	Elements of $G_0(\boldsymbol{q})$	Classification
$\boldsymbol{q}_7 = 0$	$2/m$	h_1, h_3, h_{25}, h_{27}	$5A_g + 4B_g + 4A_u + 5B_u$
$\boldsymbol{q}_1 = \mu_1\boldsymbol{b}_1 + \mu_3\boldsymbol{b}_3$	m	h_1, h_{27}	$10A' + 8A''$
$\boldsymbol{q}_{12} = \frac{1}{2}\boldsymbol{b}_3$	$2/m$	h_1, h_3, h_{25}, h_{27}	$5A_g + 4B_g + 4A_u + 5B_u$
$\boldsymbol{q}_{13} = \frac{1}{2}\boldsymbol{b}_1$			
$\boldsymbol{q}_3 = \mu_2\boldsymbol{b}_2$	2	h_1, h_3	$9A + 9B$
$\boldsymbol{q}_{11} = \frac{1}{2}\boldsymbol{b}_2$	$2/m$	h_1, h_3, h_{25}, h_{27}	$9E$

Table 3. Irreducible multiplier representations of some point groups $G_0(\boldsymbol{q})$ of wavevectors for the $P2_1/m$ space group.

$G_0(\boldsymbol{q}_7), G_0(\boldsymbol{q}_{12}), G_0(\boldsymbol{q}_{13})$ representation	h_1	h_3	h_{25}	h_{27}
A_g	1	1	1	1
B_g	1	-1	-1	1
A_u	1	1	-1	-1
B_u	1	-1	1	-1

$G_0(\boldsymbol{q}_1), G_0(\boldsymbol{q}_3)$ representation	$G_0(\boldsymbol{q}_1)$: $G_0(\boldsymbol{q}_3)$	h_1 h_1	h_{27} h_3
A' A		1	1
A'' B		1	-1

$G_0(\boldsymbol{q}_{11})$ representation	h_1	h_3	h_{27}	h_{25}
E	1 0 0 1	1 0 0 -1	0 1 -1 0	0 1 1 0

with respect to the condition of molecule electroneutrality. Thus, the constraints for the crystal potential are

$$\left.\frac{\partial\Phi}{\partial U^i_\alpha(lK)}\right|_0 = 0, \quad \frac{\partial\Phi}{\partial S_{\alpha\beta}} = 0, \quad \sum_{K,k} Z_{Kk} = 0, \tag{4}$$

where $U^i_\alpha(lK)$ is a displacement of molecule K in the unit cell l; α is the Cartesian components X, Y and Z; i refers to the translation (t) or rotation (r); $S_{\alpha\beta}$ is a macroscopic strain.

At the same time, we suppose that *a priori* the quantum particle proton located on the hydrogen bond O–H...O cannot be taken into account directly in the quasi-harmonic approximation. Therefore, the influence of the protons is taken into consideration indirectly by means of unequal values of the effective charges Z_{Kk} and radii R_{Kk} of oxygen ions in H_2PO_4 groups. With the help of *ab initio* calculations within the extended Huckel method it was shown [27] that the charges and radii of oxygen ions in the H_2PO_4 group depend on proton localization on the O–H...O bond in one of the minima of a double-well type potential in which the proton moves.

Proceeding from the aforesaid, we have used the following values of the model parameters $Z(\mathrm{Cs}) = 1.18$, $Z(\mathrm{P}) = 0.34$, $Z(\mathrm{O_1}) = -0.39$, $Z(\mathrm{O_2}) = -0.41$, $Z(\mathrm{O_3}) = Z(\mathrm{O_4}) = -0.36$; $R(\mathrm{Cs}) = 2.83$, $R(\mathrm{P}) = 1.0$, $R(\mathrm{O_1}) = 1.36$, $R(\mathrm{O_2}) = 1.32$, $R(\mathrm{O_3})R(\mathrm{O_4}) = 1.44$. The charge $Z(\mathrm{O_1})$ is smaller than $Z(\mathrm{O_2})$ because the protons on the bonds $\mathrm{O_1}$–H...$\mathrm{O_2}$ are localized near the oxygen ions $\mathrm{O_1}$ at all temperatures. The charges $Z(\mathrm{O_3})$, $Z(\mathrm{O_4})$ and radii $R(\mathrm{O_3})$, $R(\mathrm{O_4})$ are equal, respectively, because the protons on the bonds $\mathrm{O_3}$–H...$\mathrm{O_4}$ tunnel between the two possible off-centre equivalent positions in the PE phase.

Therefore, in reality the lattice dynamics of a crystal which consists of the Cs^+ and $(PO_4)^-$ ions with indirect consideration of the proton influence is studied.

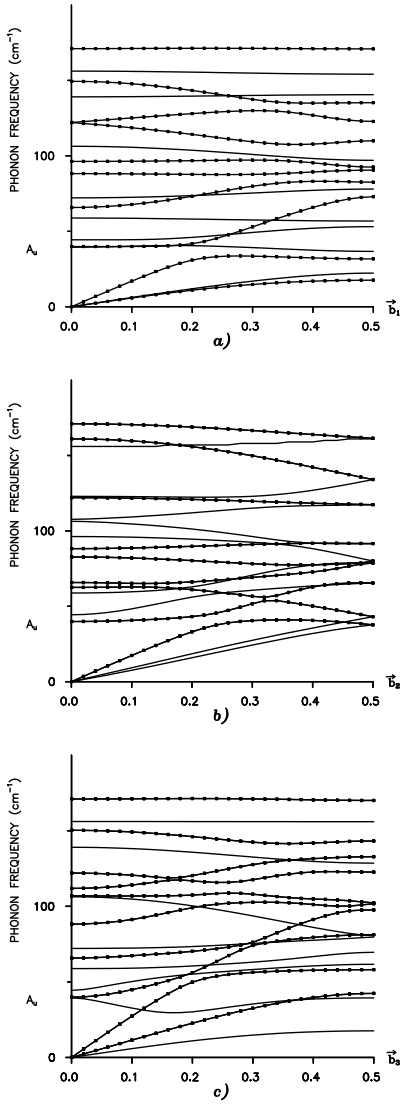

Figure 3. The phonon dispersion relations in a CsH_2PO_4 crystal in the PE phase at room temperature and atmospheric pressure along the following directions: a) $\boldsymbol{b}_1$, b) $\boldsymbol{b}_2$, c) $\boldsymbol{b}_3$.

5. Results and discussion

5.1. Phonon dispersion relations in CDP

The lattice dynamics calculation of the CDP crystal is carried out by means of the program DISPR [6] which has been modified by us in order to use the group-theory information to a greater extent. Figure 3 shows the calculated phonon dispersion relations along the directions $\boldsymbol{b}_1$, $\boldsymbol{b}_3$ ($\boldsymbol{q}_7 = 0 \rightarrow \boldsymbol{q}_1 = \mu_1\boldsymbol{b}_1 + \mu_3\boldsymbol{b}_3 \rightarrow \boldsymbol{q}_{13} = \frac{1}{2}\boldsymbol{b}_1$ or $\boldsymbol{q}_{12} = \frac{1}{2}\boldsymbol{b}_3$) and ($\boldsymbol{q}_7 = 0 \rightarrow \boldsymbol{q}_3 = \mu_2\boldsymbol{b}_2 \rightarrow \boldsymbol{q}_{11} = \frac{1}{2}\boldsymbol{b}_2$). The compatibility relations between the IMRs along these directions are presented in table 4.

Table 4. Compatibility relation between the irreducible multiplier representations along the $\boldsymbol{b}_1$, $\boldsymbol{b}_2$ and $\boldsymbol{b}_3$ directions in CsH_2PO_4 in the PE phase.

$\boldsymbol{q}_7 = 0$ $\boldsymbol{q}_7 = 0$	$\boldsymbol{q}_1 = \mu_1\boldsymbol{b}_1$ $\boldsymbol{q}_1 = \mu_3\boldsymbol{b}_3$	$\boldsymbol{q}_{13} = \frac{1}{2}\boldsymbol{b}_1$ $\boldsymbol{q}_{12} = \frac{1}{2}\boldsymbol{b}_3$	$\boldsymbol{q}_7 = 0$	$\boldsymbol{q}_3 = \mu_2\boldsymbol{b}_2$	$\boldsymbol{q}_{11} = \frac{1}{2}\boldsymbol{b}_2$
A_g B_g	A'	A_g B_g	A_g B_g	A	E
A_u B_u	A''	A_u B_u	A_u B_u	B	

The accuracy of the calculation was controlled at different stages by the correspondence of the calculated dynamical matrix $D(\boldsymbol{q})$ to the one determined theoretically by means of general symmetry requirements [18]. As one can see from figure 3, at the boundary of the BZ at point $\boldsymbol{q}_{11} = \frac{1}{2}\,\boldsymbol{b}_2$, the phonon modes become two-fold degenerate. This is a consequence of two-dimensionallity of the irreducible multiplier representation E of the group $G_0(\boldsymbol{q}_{11})$. Note, that the time-reverse symmetry does not require any additional degeneracy for all the considered cases ($\boldsymbol{q}_7$, $\boldsymbol{q}_1$, $\boldsymbol{q}_{12}$, $\boldsymbol{q}_{13}$, $\boldsymbol{q}_3$, $\boldsymbol{q}_{11}$).

The disagreement in frequencies while approaching the centre of the BZ from different directions can be explained by LO – TO splitting. Only polar modes which transform according to the IMRs A_u and B_u possess LO – TO splitting. It follows from the eigenvectors analysis that the vibrations propagating along the $\boldsymbol{b}_1$ and $\boldsymbol{b}_3$ directions are purely transverse (A_u symmetry) or quasi-transverse (B_u symmetry). At the same time, the modes propagating along the $\boldsymbol{b}_2$ direction are purely longitudinal (A_u symmetry) or purely transverse (B_u symmetry). Therefore, at $\boldsymbol{b}_2 \rightarrow 0$, the modes of A_u symmetry have larger frequencies as compared with those when $\boldsymbol{b}_1 \rightarrow 0$ or $\boldsymbol{b}_3 \rightarrow 0$ ($\omega_{\mathrm{LO}} > \omega_{\mathrm{TO}}$). On the contrary, the frequencies of the B_u symmetry at $\boldsymbol{b}_2 \rightarrow 0$ are smaller than the frequencies at $\boldsymbol{b}_1 \rightarrow 0$ and $\boldsymbol{b}_3 \rightarrow 0$, because the modes along the $\boldsymbol{b}_1$ and $\boldsymbol{b}_3$ directions are quasi-transverse and have some longitudinal components.

Table 5. Comparison of the experimental and theoretical values of external modes frequencies in the centre of the BZ in CsH_2PO_4.

representation	experiment (cm^{-1})		calculation (cm^{-1})
	Raman	IR	
A_g	43		40
	49		45
	75		88
	118		122
	219		172
B_g	45		44
	61		59
	110		106
	234		157
A_u		acoustic	acoustic
		38	39, TO
			61, LO
		74	72, TO
			82, LO
		100	139, TO
			161, LO
B_u		acoustic	acoustic
		acoustic	acoustic
			97, QTO*, $\boldsymbol{q} = (0.001, 0, 0)$
		76	96, TO, $\boldsymbol{q} = (0, 0.001, 0)$
			106, QTO, $\boldsymbol{q} = (0, 0, 0.001)$
			122, QTO, $\boldsymbol{q} = (0.001, 0, 0)$
		106	108, TO, $\boldsymbol{q} = (0, 0.001, 0)$
			112, QLO, $\boldsymbol{q} = (0, 0, 0.001)$
			149, QTO, $\boldsymbol{q} = (0.001, 0, 0)$
		146	123, TO, $\boldsymbol{q} = (0, 0.001, 0)$
			150, QLO, $\boldsymbol{q} = (0, 0, 0.001)$

*QTO, quasi-transverse optical mode
OLO, quasi-longitudinal optical mode

Comparison of the calculated phonon frequencies in the centre of the BZ ($\boldsymbol{q}_7 = 0$) with those obtained from Raman and IR investigations [19] is presented in table 5. For most of the calculated frequencies, a good agreement with the corresponding experimental results is obtained.

Table 6. The components S_{ij} of the elastic compliance matrix in CsH_2PO_4 at $T = 293$ K (according to Prewer et al. (1985))

ij	$S_{ij}(\mathrm{GPa})^{-1}$	ij	$S_{ij}(\mathrm{GPa})^{-1}$
11	1.82	12	-0.219
22	0.103	13	-1.17
33	0.772	15	0.249
44	0.133	23	0.138
55	0.450	25	-0.150
66	0.117	35	-0.181
		46	0.033

The calculation of the external phonon dispersion relation along the $\boldsymbol{b}_1$ direction attracts special interest since the PT into the AFE phase occurs in a CDP crystal at some values of temperature and hydrostatic pressure. Usually, such a PT is related to the external mode condensation at the BZ boundary at point $\boldsymbol{q}_{13} = \frac{1}{2}\boldsymbol{b}_1$. With the help of group theory consideration [17], one can show that the IMR A_u is responsible for the AFE PT in a CDP crystal with the symmetry change $P2_1/m \rightarrow P2_1/\alpha$. The same IMR A_u is responsible for the PT into the FE phase (space group $P2_1$). This PT is caused by the external mode condensation in the centre of the BZ.

The phonon spectra calculation of a CDP crystal at different values of temperature and hydrostatic pressure was carried out. Moreover, we remained within the framework of the quasi-harmonic approximation at specific values of T and P. The influence of interatomic anharmonicity on lattice dynamics is taken into consideration indirectly through the change of the lattice parameters a, b and c, which were determined from the experimental data of thermal expansion and ultrasonic measurements. We assumed that the temperature and hydrostatic pressure influence the lattice parameters only (without a change of fractional atomic coordinates in a unit cell) according to the next linear laws:

$$a = (1 - K_a P)a_T, \quad b = (1 - K_b P)b_T, \quad c = (1 - K_c P)c_T, \tag{5}$$

where K_a, K_b and K_c are linear compressibility components along the a, b and c axes, respectively, at the applied hydrostatic pressure P; a_T, b_T and c_T are the lattice parameters at temperature T.

The linear compressibility K_{lmn} of a monoclinic crystal with the $P2_1/m$ symmetry along the given direction $[l, m, n]$ in the Cartesian coordinate system X, Y and Z is written as [23]

$$\begin{aligned} K_{lmn} \;=\; & (S_{11} + S_{12} + S_{13})l^2 + (S_{12} + S_{22} + S_{23})m^2 \\ & + (S_{13} + S_{23} + S_{33})\, n^2 + (S_{16} + S_{26} + S_{36})lm, \end{aligned} \tag{6}$$

here S_{ij} are components of the elastic compliance matrix which is inverse to the elastic constant matrix C_{ij}. The values of S_{ij} components for the CDP crystal,

determined at room temperature by the ultrasonic waves velocities measurements [24], are presented in table 6.

Thus, the components of the CDP crystal linear compressibility along the crystallographic a, b and c axes have the following values: $K_a = 0.022$, $K_b = -0.260$ and $K_c = 0.390$. At the same time, we assume that the linear compressibility is independent of both the temperature and hydrostatic pressure.

To determine the thermal dependence of the lattice parameters a, b and c, the dilatometric investigations of monodomain specimen have been carried out. The linear thermal expansion ($\Delta 1/1$) observed along the a^*, b and c directions as a function of temperature, where $a^* \perp (b, c)$, is shown in figure 4. As one can see, $\Delta 1/1$ along the b and c axes are essentially larger than $\Delta 1/1$ along a^* direction. This can indicate a quasi-layer nature of the CDP crystal along the (b, c) plane. In other words, interactions between the ions within the same layer are to a great extent larger than interactions between the ions from different layers. The perfect cleavage that occurs along the (b, c) plane confirms a relative weakness of interlayer forces. Therewith, the linear thermal expansion along the c axis increases with the temperature decrease, i.e. the CDP crystal expands along this axis at cooling. The thermal expansion coefficient a along c axis becomes negative. This unusual behaviour of the coefficient a is considered in detail in [37].

5.2. Phonon dispersion relations in a CDP crystal at different values of temperature and hydrostatic pressure

Using the data of thermal expansion (figure 4) and linear compressibility (table 6) of a CDP crystal, with the help of expression (5) it is easy to obtain the lattice parameters at various values of T and P. The calculated dispersion relations for external phonon modes of the B symmetry ($G_0\boldsymbol{q}_1$) along the $\boldsymbol{b}_1$ direction at different values of T and P are presented in figure 5. As one can see, at increasing the hydrostatic pressure and decreasing the temperature, a lowering of most of the phonon branches is observed. At $T = 130$ K and $P = 241$ MPa, the lower optic phonon branch of the A_u symmetry falls to zero in the centre of the BZ (at room temperature and atmospheric pressure the value of this optic mode is 39 cm^{-1}. This implies that in a CDP crystal the PT into the PE phase must occur.

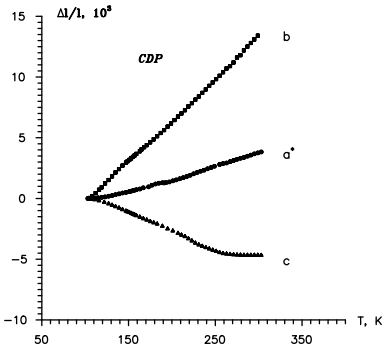

Figure 4. The linear thermal expansion along the orthonormal a^*, b, and c axes of a CsH_2PO_4 crystal.

At the same time there occur such displacements of structural units of the crystal to new equilibrium sites which define the structure of the PE phase. These displacements, determined from the analysis of the eigenvector corresponding to the soft phonon mode A_u, are schematically presented in figure 6. As follows from this figure, the Cs^+ and $(PO_4)^-$ ions shift along the b axis in opposite directions

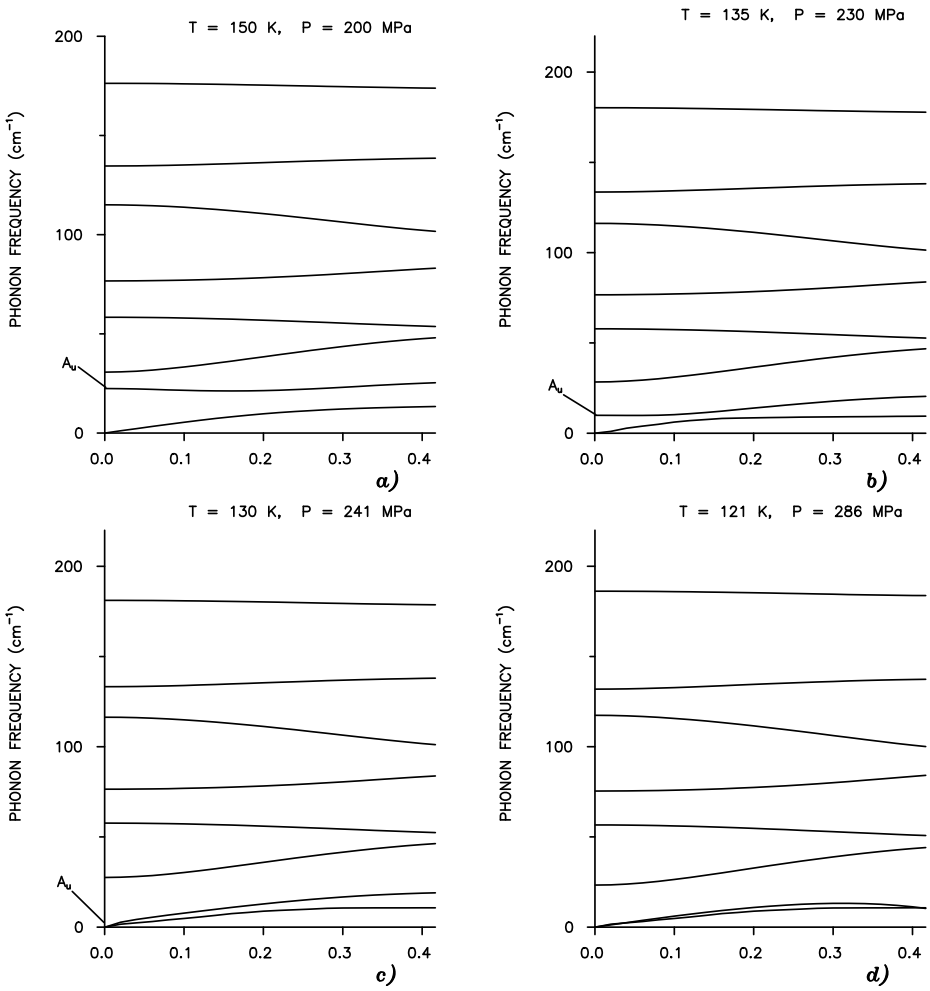

Figure 5. The dispersion relations of phonon modes of the B symmetry along the $\boldsymbol{b}_1$ direction in a CsH_2PO_4 crystal at different values of temperature and hydrostatic pressure:
a) $T = 150$ K, $P = 200$ MPa; b) $T = 135$ K, $P = 230$ MPa;
c) $T = 130$ K, $P = 241$ MPa; d) $T = 121$ K, $P = 286$ MPa.

with simultaneous PO_4 group rotation in the *ac*-plane. The calculated displacements of structural units both translational and rotational are in good qualitative agreement, with neutron scattering data [12].

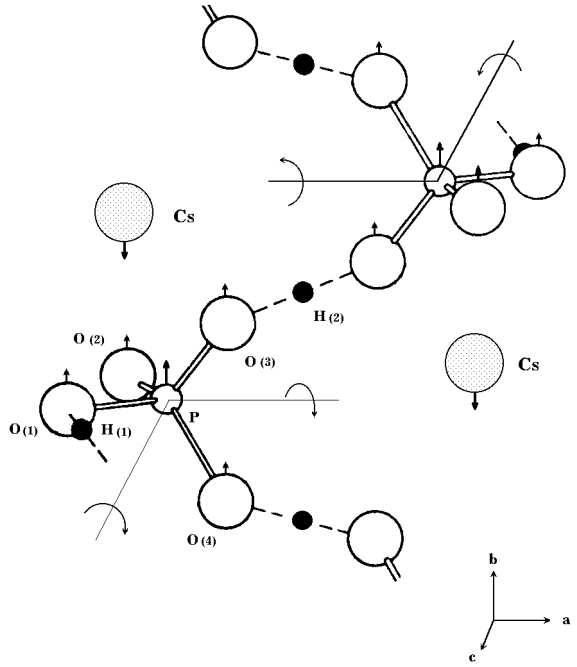

Figure 6. Schematic representation of ions displacements corresponding to the ferroactive A_u soft phonon mode determined from the eigenvector analysis.

Variation of lattice parameters with temperature and hydrostatic pressure is accompanied by a change of effective charges and radii. For preserving the equilibrium conditions (4) it is necessary to change the model parameters to the following values $Z(\mathrm{Cs}) = 1.21$, $Z(\mathrm{P}) = 0.33$, $Z(\mathrm{O}_1) = -0.40$, $Z(\mathrm{O}_2) = -0.42$, $Z(\mathrm{O}_3) = -0.36$; $R(\mathrm{Cs}) = 2.85$, $R(\mathrm{P}) = 1.0$, $R(\mathrm{O}_1) = 1.35$, $R(\mathrm{O}_2) = 1.31$, $R(\mathrm{O}_3) = R(\mathrm{O}_4) = 1.44$ at $T = 130$ K and $P = 241$ MPa.

In figure 7a, the dispersion relation of the soft phonon mode A_u in the plane ($\boldsymbol{b}_1$, $\boldsymbol{b}_3$) at $T = 130$ K and $P = 241$ MPa is depicted. As one can see from the $P - T$ phase diagram (figure 2), the PT into the FE phase takes place at $T = 130$ K and $P = 251$ MPa, i.e. the calculated values of temperature $T = 130$ K and hydrostatic pressure $P = 241$ MPa are in good agreement with the experimental data. For other values of T, there is no good coincidence between the experimental and the calculated values of P at which the PT into the FE phase occurs. It should be noted that the calculated frequencies of external phonon modes are more sensitive to the influence of hydrostatic pressure on the lattice parameters than to the temperature influence. So, at $T = 121$ K and $P = 286$ MPa (an experimental value of hydrostatic pressure obtained from the $P-T$ phase diagram for $T = 121$ K is $P = 370$ MPa), the lowering to zero of the same lower optic

phonon branch of the A_u symmetry, active at PT into the FE phase, takes place at the BZ boundary at point $\boldsymbol{q}_{13} = \frac{1}{2}\boldsymbol{b}_1$ (figure 5). In other words, the PT into the AFE phase, accompanied by the unit cell doubling along the a axis, must occur in a CDP crystal at some values of T and P. Here the displacements of the crystal structural units to new equilibrium sites of the AFE phase are similar to those presented in figure 6, only they are opposite in the neighbouring cells. In figure 7 the calculated dispersion relation of the soft phonon mode A_u in the plane ($\boldsymbol{b}_1$, $\boldsymbol{b}_3$) at $T = 121$ K, $P = 286$ MPa (i.e. at the PT into the AFE phase) is presented.

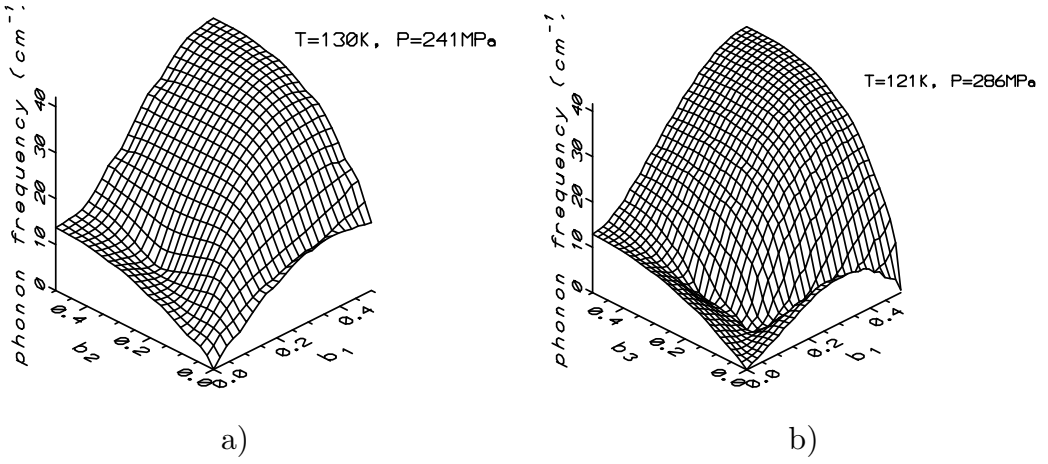

a) b)

Figure 7. The dispersion relation of the A_u soft phonon mode in the ($\boldsymbol{b}_1, \boldsymbol{b}_3$) plane at a) $T = 130$ K and $P = 241$ MPa; b) $T = 121$ K and $P = 286$ MPa.

6. Conclusions

In this paper we have reported the results of lattice-dynamical calculations of a CDP crystal based on the rigid molecular-ion model which includes the Coulomb and short-range interactions. The protons on hydrogen bonds in the quasi-harmonic approximation have not been taken into account immediately but indirectly by means of choice of the unequal values of effective charges and radii of oxygen ions in H_2PO_4 groups. This approach provides a reasonable explanation of the observed Raman and IR data for a CDP crystal in the external modes region where the effects of internal vibrations are not expected to be felt. In the case when anharmonic particles of the protons were taken into consideration immediately as hard atoms (e.g., Cs, P, or O) there was a significant aggravation of lattice equilibrium conditions and appearance of unphysical results (the phonon frequencies with imaginary values).

The lattice dynamics calculation of a CDP crystal at different values of temperature and hydrostatic pressure was carried out. Thereat, we supposed that in the quasi-harmonic approximation the influence of T and P would be displayed only through the change of the lattice parameters a, b and c. For this purpose,

dilatometric investigations of a CDP crystal were performed. Using the ultrasonic waves velocities measurements [24], the values of linear compressibility along the a, b and c axes were obtained. This enabled us to calculate the phonon spectra of CDP at various values of T and P. At decreasing temperature and increasing hydrostatic pressure the lowering of most of the phonon branches was observed. At $T = 130$ K and $P = 241$ MPa, the lower optic phonon branch of the A_u symmetry falls to zero in the centre of the BZ ($\boldsymbol{q}_7 = 0$). At $T = 121$ K and $P = 286$ MPa, the same lower optic phonon branch tends to zero at the boundary of the BZ at point $\boldsymbol{q}_{13} = \frac{1}{2}\boldsymbol{b}_1$. In other words, the obtained results qualitatively show that the PT in a CDP crystal takes place either into the FE phase (condensation of the A_u mode in the BZ centre) or into the AFE phase (condensation of the A_u mode at the BZ boundary) depending on a correlation of interatomic forces which depend on the temperature and hydrostatic pressure. It confirms once more an extremely important role of a proton subsystem in phase transitions in the compounds of this type.

References

1. Anisimova V.N., Yakushkin E.D, Majszchyk J. Acoustic and dielectric properties of quasi-one-dimensional ferroelectric CsH_2PO_4 in an external electric field. // Journ. Mater. Science Lett., 1993, vol. 12, No. 3, p. 588–590.
2. Arai M., Yagi T., Sakai A., Komukae M., Osaka T., Makita Y. Elastic instability in the ferroelastic phase transition of TlH_2PO_4 studied by Brillouin scattering. // J. Phys. Soc. Japan, 1990, vol. 59, No. 2, p. 1285–1292.
3. Blinc R., Žekš B. Ferroelektrics and antiferroelectrics. Moskow, Mir, 1975 (in Russian).
4. Boyer L.L., Hardy J.R. Static equilibrium conditions for rigid-ion crystals. // Phys. Rev. B., 1973, vol. 7, p. 2886–2888.
5. Brandt N.B., Chookov S.G., Kulbachinskii V.A., Smirnov P.S., Strukov B.A. // Fiz. Tverd. Tela, 1986, vol. 28, p. 3159 (in Russian).
6. Chaplot S.L. A computer program for external modes in complex ionic crystals (the rigid molecular-ion model). Report N BARC 972 Bhabha Atomic Research Centre (Bombay), 1978.
7. Deguchi K., Nakamura E., Okaue E., Aramaki N. Effects of deuteration on the dielectric properties of ferroelectric CsH_2PO_4. II. Dynamic dielectric properties. // J. Phys. Soc. Japan, 1982, vol. 51, p. 3575–3582.
8. Fillaux F., Marchon B., Novak A. Shape of Raman OH stretching band and proton dynamics in CsH_2PO_4. // Chem. Phys., 1984, vol. 86, p. 127–136.
9. Frazer B.C., Semmingsen D., Ellenson W.D., Shirane G. One-dimensional ordering in ferroelectric CsD_2PO_4 and CsH_2PO_4 as studied with neutron scattering. // Phys. Rev., 1979, vol. 20, p. 2745–2755.
10. Hagiwara T., Itoh K., Nakamura E., Komukae M., Makita Y. Structure of monoclinic rubidium dideuteriumphosphate, RbD_2PO_4, in the intermediate phase. // Acta Cryst., 1984, vol. C40, p. 718–720.
11. Itoh K., Hagiwaga T., Nakamura E. Order-disorder type phase transition in ferroelectric CsD_2PO_4 studied by X-ray structure analysis. // J. Phys. Soc. Japan, 1983, vol. 52, p. 2626–2629.

12. Iwata Y., Koyano N., Shibuya I. A neutron diffraction study of the ferroelectric transition of CsH_2PO_4. // J. Phys. Soc. Japan, 1980, vol. 49, p. 304–307.
13. Kasahara M., Aoki M., Tatsuzaki I. Raman study of the phase transition in CsH_2PO_4 and CsD_2PO_4. // Ferroelectrics, 1984, vol. 55, p. 47–50.
14. Kityk A.V., Shchur Ya.I., Lutsiv-Shumskii L.P., Vlokh O.G. On the acoustic properties of CsD_2PO_4 and RbD_2PO_4 crystals near phase transitions under hydrostatic pressure. // J. Phys.: Condens. Matter, 1994, vol. 6, p. 699–712.
15. Kovalev O.V. Irreducible Representations of the Space Groups. New York, Gordon and Breach Science Publishers, 1965.
16. Lifshits I.M. About thermal properties of chain-type and layer-type structures at low temperatures. // Zhurn. Eksper. Teoret. Fiz., 1952, vol. 22, p. 475–486.
17. Liubarskii G.Ya. The Application of Group Theory in Physics, New York, Pergamon Press, 1960.
18. Maradudin A.A., Vosko S.H. Symmetry properties of the normal vibrations of a crystal. // Rev. Mod. Phys., 1968, vol. 40, p. 1–76.
19. Marchon E. Etude vibrationelle des transitions de phase d'un ferroelectrique pseudo-unidimensionnel CsH_2PO_4, Paris, These de doctorat d'etat, 1983.
20. Marchon B., Novak A. Antiferroelectric fluctuations in CsH_2PO_4 and Raman spectroscopy. // Ferroelectrics, 1984, vol. 55, p. 55–58.
21. Matsunaga H., Itoh K., Nakamura E. X-ray structural study of ferroelectric cesium dihydrogen phosphate at room temperature. // J. Phys. Soc. Japan, 1980, vol. 48, p. 2011–2014.
22. Nelmes R.J., Choudhary R.N.P. Structural studies of the monoclinic dihydrogen phosphates: a neutron-diffraction study of paraelectric CsH_2PO_4. // Sol. Stat. Commun., 1978, vol. 26, p. 823–826.
23. Nye J.F. Physical Properties of Crystals, Oxford, Clarendon, 1967
24. Prawer S., Smith T.F., Finlayson. The room temperature elastic behaviour of CsH_2PO_4. // Aust. Journ. Phys., 1985, vol. 38, p. 63–83.
25. Schuele P.J. , Thomas R. A structural study of the high-pressure antiferroelectric phase of CsH_2PO_4. // Japan Journ. Appl. Phys., 1985, vol. 24, p. 935–937.
26. Seliger J., Zagar V., Blinc R., Schmidt V.H. O^{17} study of the antiferroelectric phase transition in TlH_2PO_4. // J. Chem. Phys., 1988, vol. 88, p. 3260–3262.
27. Stetsiv R. Electron states and optical effects in the KH_2PO_4-type crystals with hydrogen bonds. Thesis on Doctor of Philosophy degree, Lviv, 1993.
28. Shin S., Ishida A., Yamakami T., Fujimura T., Ishigame M. Central mode in hyber-Raman spectra of the quasi-one-dimensional hydrogen-bonded ferroelectric CsH_2PO_4. // Phys. Rev. B, 1987, vol. 35, p. 4455–4461.
29. Suzuki S., Arai K., Sumita M., Makita Y. X-ray diffraction study of monoclinic RbD_2PO_4. // J. Phys. Soc. Japan, 1983, vol. 7, p. 2394–2400.
30. Ti S.S., Rumble S., Ninio F. Infrared spectra of paraelectric and ferroelectric CsH_2PO_4. // Sol. Stat. Commun., 1982, vol. 44, p. 129–135.
31. Yasuda N., Kawai J. Dielectric dispersion associated with the de-electric-field-enforced ferroelectric phase transition in the pressure-induced antiferroelectric CsH_2PO_4. // Phys. Rev. B, 1990, vol. 42, p. 4893–4896.
32. Yasuda N., Okamoto M., Shimuzu H., Fujimoto S., Yoshino K. , Inuishi Y. Pressure-induced antiferroelectricity in ferroelectric CsH_2PO_4. // Phys. Rev. Lett., 1978, vol. 41, p. 1311–1313.

33. Youngblood R., Frazer B.C., Eckert J., Shirane G. Neutron scattering study of pressure dependence of short-range order in CsD_2PO_4. // Phys. Rev. B, 1980, vol. 22, p. 228–235.
34. Uesu Y., Kobayashi J. Crystal structure and ferroelectricity of cesium dihydrogen phosphate CsH_2PO_4. // Phys. Stat. Sol. (a), 1976, vol. 34, p. 475–481.
35. Ushio S. Temperature variations of optical indicatrix and birefringence in ferroelectric CsH_2PO_4. // J. Phys. Soc. Japan, 1984, vol. 53, p. 3242–3249.
36. Venkataraman G., Sahni V.C. External vibration in complex crystals. // Rev. Mod. Phys., 1970, vol. 42, p. 409–470.
37. Vlokh O.G. Shchur Ya.I., Hirnyk I.S., Klymiv I.M. About thermal expansion of RbD_2PO_4,CsH_2PO_4 and CsD_2PO_4. // Fiz. Tverd. Tela, 1994, vol. 36, p. 2890–2895 (in Russian).
38. Wada M., Sawada A., Ishibashi Y. Some high-temperature properties and the Raman scattering spectra of CsH_2PO_4. // J. Phys. Soc. Japan, 1979, vol. 47, p. 1571–1547.

Граткова динаміка моноклінного кристала CsH_2PO_4

Я.І.Щур [1], Р.Р.Левицький [2], О.Г.Влох [1], А.В.Кітик [1], Й.М.Височанський [3], А.А.Грабар [3]

[1] Інститут фізичної оптики,
290005 Львів, вул. Драгоманова, 23

[2] Інститут фізики конденсованих систем НАН України,
290011 Львів, вул. Свєнціцького, 1

[3] Ужгородський державний університет,
294000 Ужгород, вул. Підгірна, 46

Отримано 19 листопада 1997 р.

В рамках моделі жорстких іонів обчислюються фононні дисперсійні співвідношення в параелектричній фазі кристала CsH_2PO_4. Фононні спектри отримані в квазігармонічному наближенні для різних значень температури і гідростатичного тиску. Виявлено конденсацію зовнішньої фононної гілки A_u в центрі і на границі зони Бріллюена.

Ключові слова: *динаміка гратки, м'яка мода, структурний фазовий перехід, фононний спектр*

PACS: *63.20.-e, 63.20.Dj*